Title: Impact of Ferumoxytol Magnetic Resonance Imaging on the Rhesus Macaque Maternal-Fetal Interface

Running Title: Ferumoxytol MRI in Rhesus Macaque Pregnancy

Summary Sentence: Ferumoxytol magnetic resonance imaging for non-invasive pregnancy monitoring of the rhesus macaque does not impact histopathology or iron content of the maternal-fetal interface.

Keywords: ferumoxytol, imaging, iron nanoparticles, MRI, placenta, pregnancy, primates

Sydney M. NGUYEN[1,2], Gregory J. WIEPZ[1], Michele SCHOTZKO[1], Heather A. SIMMONS[1], Andres MEJIA[1], Kai D. LUDWIG[3], Ante ZHU[4,5], Kevin BRUNNER[1,6], Diego HERNANDO[3,5], Scott B. REEDER[3,4,5,6,7], Oliver WIEBEN[3,5], Kevin JOHNSON[3,5], Dinesh SHAH[2], Thaddeus G. GOLOS[1,2,8]

[1]Wisconsin National Primate Research Center (WNPRC), Madison, Wisconsin, USA

[2]Obstetrics & Gynecology, University of Wisconsin Madison School of Medicine, Madison, Wisconsin, USA

[3]Medical Physics, University of Wisconsin Madison, Madison, Wisconsin, USA

[4]Biomedical Engineering, University of Wisconsin Madison, Madison, Wisconsin, USA

[5]Radiology, University of Wisconsin Madison, Madison, Wisconsin, USA

[6]Emergency Medicine, University of Wisconsin Madison, Madison, Wisconsin, USA

[7]Medicine, University of Wisconsin Madison, Madison, Wisconsin, USA

[8]Comparative Biosciences, University of Wisconsin Madison, Madison, Wisconsin, USA

Support: The National Institutes of Health (NIH) Grants U01HD087216 to D. Shah and O. Wieben, University of Wisconsin Institute for Clinical and Translational Research (UW ICTR) UL1 TR000427 (to M. Drezner), TL1 TR000429 (to KDL), UW Radiological Sciences Training Grant T32 CA009206 (to KDL), K24 DK102595 (to SBR), R01 DK011651 (to SBR), R01 DK117354 (to DH), Endocrinology-Reproductive Physiology Training Grant T32 HD041921 (to SMN), and P51 OD011106 (to the WNPRC).

*__Correspondence to:__ Thaddeus G. Golos, Ph.D., 1223 Capitol Ct., Madison, Wisconsin, USA 53715-1299. E-mail: golos@primate.wisc.edu

Abstract

Ferumoxytol is a superparamagnetic iron oxide nanoparticle (SPION) used off-label as an intravascular magnetic resonance imaging (MRI) contrast agent. Additionally, ferumoxytol-uptake by macrophages facilitates detection of inflammatory sites by MRI through ferumoxytol-induced image contrast changes. Therefore, ferumoxytol-enhanced MRI holds great potential for assessing vascular function and inflammatory response, critical to determine placental health in pregnancy. This study sought to assess the fetoplacental unit and selected maternal tissues, pregnancy outcomes, and fetal well-being after ferumoxytol administration. In initial developmental studies, pregnant rhesus macaques were imaged with and without ferumoxytol administration. Pregnancies went to term with vaginal delivery and infants showed normal growth rates compared to control animals born the same year that did not undergo MRI. To determine the impact of ferumoxytol on the maternal-fetal interface, fetal well-being, and pregnancy outcome, four pregnant rhesus macaques at ~100 gd (gestational day) underwent MRI before and after ferumoxytol administration. Collection of the fetoplacental unit and selected maternal tissues was performed 3-4 days following ferumoxytol administration. A control group that did not receive ferumoxytol or MRI was used for comparison. Iron levels in fetal and maternal-fetal interface tissues did not vary between groups. There was no significant difference in tissue histopathology with or without exposure to ferumoxytol, and no effect on placental hormone secretion. Together, these results suggest that the use of ferumoxytol and MRI in pregnant rhesus macaques will not introduce a detectable risk to the mother or fetus at the time of imaging or up to one year following normal vaginal delivery.

Introduction

In the hemochorial human and nonhuman primate placenta, maternal intervillous blood bathes the placental villi, allowing oxygen and nutrient transfer to the fetal blood circulating within the capillaries of the villous stroma. Pregnancy complications may stem from maladaptation of maternal vessels causing insufficient placental perfusion, leading to macrophage recruitment, cytokine release, and hypoxia at the maternal-fetal interface (MFI). Compromised intervillous flow is associated with adverse pregnancy outcomes [1-4]: insufficient placental perfusion could result in fetal growth restriction, preeclampsia, and pregnancy loss. The ability to identify abnormal uteroplacental vascular adaptation, compromised perfusion, and attendant inflammation could be valuable in identifying at-risk pregnancies before clinical manifestations.

Currently, ultrasound is the most commonly used method to assess fetal growth. It is also used to detect umbilical and uteroplacental blood flow abnormalities, but only indirectly through velocity waveform analysis. Further, ultrasound lacks the ability to detect immune cell homing to the MFI that may precede adverse pregnancy outcomes. Magnetic resonance imaging (MRI) can provide high-resolution anatomic and functional information including blood velocities and flow, perfusion, and oxygenation to characterize placental implantation site, visualize maternal pelvic structures, and diagnose abnormally aggressive trophoblast invasion or placental abruption [5]. In many clinical applications, gadolinium-based contrast agents (GBCAs) are used to quantify tissue perfusion and perform high-resolution angiography [6]. In the non-human primate, gadolinium MRI has been used to investigate spiral artery and perfusion domain (cotyledon) location, and quantify placental perfusion [7,8], the latter of which has also been achieved in humans [9]. However, GBCAs have been shown to cross the placenta into the fetus with

uncertainty in the long-term consequences of in utero GBCA exposure. Although there is no specific evidence that it causes teratogenic or chromosomal damage [5,10-12], the risk to the fetus of gadolinium based MR contrast agent administration remains unknown and should not be routinely provided to pregnant patients [13].

We explored an alternative approach for quantitative tissue perfusion and MR angiography in pregnancy, using the SPION ferumoxytol as a contrast agent. Ferumoxytol is approved for the treatment of iron deficiency in adults, including pregnant women. It has also emerged as an off-label MR contrast agent with favorable MR properties [14,15] that can yield high-detail angiography and functional information about the MFI non-invasively, including quantitative perfusion maps of maternal blood that allow for analysis of individual cotyledons in the placenta [16], as seen in imaging with gadolinium [7]. As such, it has high potential to identify local and global perfusion abnormalities that might be indicative of placenta pathologies..Our initial MR imaging results suggest that ferumoxytol stays within the maternal blood and does not cross the placenta into the fetal circulation immediately after ferumoxytol administration [17]. Ferumoxytol also has the potential to spatially localize inflammatory events, as the nanoparticles are taken up by activated cells of the mononuclear phagocyte system at sites of tissue inflammation, which can then be imaged after ferumoxytol in the blood space has cleared [14,18-22]. The MRI transverse relaxation rate R2* has a known linear relationship with the concentration of iron in tissues. Therefore, R2* mapping may enable localization of iron-laden macrophages, as well as quantification of their density.

Ferumoxytol has been previously used in, but is not limited to, the study of inflammation of the pancreas in patients with type-1 diabetes [22], inflammation of the lymph nodes in patients with Hodgkin lymphoma [18,21], inflammation in patients with osteomyelitis and arthritis, the

study of normal adrenal function, monitoring of kidney transplant vessel patency, monitoring intracranial aneurysms for potential rupture, and in the tracking of stem cell grafts. Application of ferumoxytol use to the MFI may be extremely valuable for the monitoring of placental dysfunction. Ferumoxytol is routinely used to treat anemia in pregnant mothers. Its safety profile and properties for MR imaging makes it a promising contrast agent to fill a gap in the non-invasive diagnosis of placental health with potential for clinical routine use. Importantly, demonstrating the safe use of ferumoxytol for placental imaging is a necessary step in this application. Therefore, the purpose of this work is to assess the feasibility of ferumoxytol administration on the MFI, fetal well-being, and pregnancy outcomes in a non-human primate model. The rhesus macaque provides an accurate experimental model of the human MFI and immune system, having hemochorial placentation, endovascular trophoblast invasion with attendant spiral artery remodeling, and chorionic villous placental architecture. We observed no negative impact from ferumoxytol injection on the histopathology at the MFI, or evidence of ferumoxytol transfer to the fetus, as assessed by iron content in MFI and fetal tissues These results demonstrate the feasible infusion of ferumoxytol in a cohort of pregnant rhesus macaques. Future work will utilize this instructive animal model with ferumoxytol-enhanced MRI to challenge experimental paradigms and understand interventions assessing placental function and pregnancy well-being.

Materials/Methods

Several aspects of the impact of ferumoxytol on the Rhesus Macaque MFI were interrogated: in vitro analysis of immune cell isolation and incubation with ferumoxytol; placental explant incubation with ferumoxytol; maternal and fetal outcomes at year post-birth for rhesus that underwent ferumoxytol MRI during pregnancy vs. controls; tissue iron content, maternal plasma analysis, and histopathology analysis in a cohort of rhesus that went fetectomy after undergoing ferumoxytol MRI.

Immune Cell Isolation and Incubation with Ferumoxytol

In vitro ferumoxytol-uptake studies using monocytes and macrophages were isolated from whole blood drawn from pregnant rhesus macaques, at approximately 100gd, as previously reported [23]. Neutrophils were isolated as previously published [24]. All three cell types were incubated in ferumoxytol (Feraheme, AMAG Pharmaceuticals, Waltham, MA) at 0, 50, 100 or 200 µg/ml for 1 hour. Additionally, there were incubations of 0 µg/ml or 200 µg/ml with activating agents (50 ng/ml phorbol-12-myristate-13-acetate (PMA; Sigma-Aldrich, St. Louis MO)) for all cell types, 750 ng/ml ionomycin (Sigma-Aldrich, St. Louis MO) for monocytes only). Following incubation, cells were washed and fixed with 2% paraformaldehyde (PFA) for visualization of iron content by Prussian Blue staining [25-27]. Cells were imaged using a Nikon Eclipse TE300 microscope with NIS-Elements image capture.

Placental Explant Incubations in Ferumoxytol

Prior to imaging experiments, placental explants were prepared from tissues obtained from untreated animals undergoing fetectomy or caesarean section in unrelated studies, during

first trimester of pregnancy or at term. Explants were incubated in ferumoxytol at 0, 100 or 200 µg/ml, diluted in DMEM/F12 with 10% fetal calf serum, for 2, 4, and 24 hours at 37°C in room air/5% CO2. Explants were fixed in 2% PFA overnight and embedded in paraffin blocks. Tissues were imaged using a Nikon Eclipse TE300 microscope with NIS-Elements image capture.

Prussian Blue Staining

To visualize cellular iron content, isolated, fixed immune cells grown on coverslips or deparaffinized rehydrated tissue sections were incubated in Prussian blue solution [25-27] for 20 minutes, washed with deionized water, and mounted with Aquapolymount (Polysciences, Warrington PA).

Care and Use of Macaques

Female rhesus macaques in the Wisconsin National Primate Center (WNPRC) breeding colony were housed with compatible males and monitored for breeding and menses. Pregnancies were confirmed and dated (+/- 2 days) based on menstrual cycle, observation of copulation, and ultrasound measurements of gestational sac and fetuses. Blood samples were collected using a needle and syringe or vacutainer system from the femoral or saphenous vein. All macaques were cared for by WNPRC staff in accordance with the regulations and guidelines outlined in the Animal Welfare Act and the Guide for the Care and Use of Laboratory Animals. This study was approved by the University of Wisconsin-Madison Graduate School Institutional Animal Care and Use Committee (IACUC).

MRI Impact on Pregnancy Outcome and Postnatal Growth

There were two imaging phases in this study. In the first phase (Supplemental Fig. 1 A), seven pregnant macaques were imaged, three with ferumoxytol and four without, to establish standard methods for anesthesia, imaging, and pilot scan settings with pregnancies proceeding to term. Infants joined the WNPRC colony and body weights during the first year of life were compared to 116 untreated macaque infants born at the WNPRC in 2016 to determine if MRI during pregnancy impacted postnatal growth. Mean and standard deviation for these colony infants were calculated at different ages, similar to the approach previously published [28]. Weights of infants exposed to MRI with or without ferumoxytol in-utero that were then born into the colony were compared to this WNPRC 2016 colony growth chart through their first year of life.

Use of IL-1b to Induce MFI Inflammation

In the second phase (Supplemental Fig. 1 B), we used a paradigm of ferumoxytol MRI following intra-amniotic injection of 10mg IL-1β (has been reported previously to increase decidual macrophage numbers and model chorioamnionitis and preterm labor [29,30]) or sterile saline (n=4) to test the efficacy of ferumoxytol detection of mononuclear phagocytes and inflammation [14,18-22] at the MFI. Untreated controls (n=4) did not receive intra-amniotic injections, ferumoxytol, or MRI. While the resulting R2* maps from IL-1β-exposed animals did not differ from those of animals receiving intra-amniotic saline (Zhu et al, under review), comparison of saline-injected and untreated animals allows determination of any impact of ferumoxytol MRI at the MFI or on the fetus.

Intra-amniotic Injection

Procedures were performed under transabdominal ultrasound guidance on the lateral aspect of the abdomen. A syringe filled with sterile saline was attached to a biopsy needle and inserted through an aseptically prepared site of the abdominal wall until the tip reached the wall of the uterus, avoiding the bowel and bladder (n=4, Supplemental Fig. 1 B). The needle was advanced into the amniotic cavity and a small amount of amniotic fluid was drawn to confirm needle placement. The contents of the syringe were then slowly injected into the amniotic cavity, and the needle was withdrawn. Following withdrawal of the needle, the insertion site in the uterus was observed by ultrasound to confirm lack of bleeding.

MRI

All animals that underwent an MRI exam, regardless of whether they also received ferumoxytol, were sedated by injection of up to 10 mg/kg ketamine, intubated, and anesthesia was maintained by inhalation of oxygen and 1.5% isoflurane. A pulse oximeter probe was placed and vital signs were monitored every 15 minutes. Animals were imaged in the right-lateral position and a respiratory bellow was placed around the animal's belly during imaging to enable respiratory-compensated imaging that minimizes motion-related artifacts. Animals that received ferumoxytol had an intravenous catheter placed for injection during imaging.

Animals that received ferumoxytol, dynamic contrast enhanced (DCE) images were acquired on a clinical 3.0T MRI system (Discovery MR750, GE Healthcare, Waukesha, WI) utilizing a 32-channel torso radiofrequency coil (Neocoil, Pewaukee, WI). Time resolved T1-weighted DCE images with 5 second temporal resolution were obtained throughout the ferumoxytol administration [17]. Ferumoxytol diluted 5:1 with normal saline was administered at 4 mg/kg body weight over a 20 second interval using a power injector, followed by a 20 ml

saline flush at the same rate. A baseline R2* MRI scan (an MRI relaxation parameter highly correlated and sensitive to detect iron concentration) was performed before ferumoxytol administration. R2* measurements were estimated in the maternal, MFI, and fetal tissues by region-of-interest analysis directly from the MRI images. Follow-up R2* MRI scans were performed on subsequent days after contrast injection to determine the persistence of ferumoxytol in various tissues. MRI acquisition parameter details can be found elsewhere [17 *and* Zhu et al, under review].

Fetectomy

At ~gd100 the fetoplacental unit was collected via hysterotomy (n=8, Supplemental Fig. 1 B). Maternal biopsies were collected aseptically during surgery and the dam recovered. The fetus was euthanized by intravenous or intracardiac injection of 50 mg/kg sodium pentobarbital. Fetal and MFI tissues were dissected for histology, iron content mass spectrometry, and protein assay.

Tissue Homogenates

Tissues collected at fetectomy (0.1-0.7g) (n=8, Supplemental Fig. 1 B) were homogenized in a Bullet Blender (Next Advance, Troy NY) at full power for 10 minutes with non-metal blending beads and 500 µL PBS. Tissue homogenate was stored at -80°C until use. A 96-well format micro BCA protein assay (Thermo Scientific, 23235) was used to determine protein concentrations in homogenates assayed for iron content according to the manufacturer's instructions.

Iron content determinations

Tissue homogenates were assayed for iron concentrations at the Wisconsin State Laboratory of Hygiene Trace Element Research Group in selected maternal, fetal, and MFI tissues via inductively coupled plasma - optical emission spectrometry [31-34]. The limit of detection is 1µg/g tissue.

Steroid Hormone Extraction and LC/MS/MS Analysis

Maternal plasma samples (450 µl) collected for multi-steroid analysis from animals that had tissues collected at fetectomy (Supplemental Fig. 1 B) were extracted and assayed as previously reported [35,36].The limit of detection is 30pg/ml for progesterone; 6pg/ml for estrone and estradiol.

Histology

Tissues collected for histology were fixed in 4% PFA overnight, 70% ethanol overnight, and routinely processed and embedded in paraffin. 5µm sections were stained with H&E and assessed by veterinary pathologists blinded to treatment groups. Tissues were evaluated for the presence or absence of physiologically significant pathologic changes, normal anatomic variations, and inflammation. Morphologic diagnoses (Supplemental Data 2) summarize these histologic findings. Organs not given a morphologic diagnosis are considered to have no significant pathologic or inflammatory changes and were scored as a 0. Severity (none=0, minimal=1, mild=2, moderate=3, severe=4) was determined by the extent and distribution of inflammation, vascular change (infarction, thrombosis, pregnancy associated vascular remodelling and/or the lack thereof), and non-vascular necrosis across the tissue section or organ

(multiple slides were necessary to evaluate the placenta). Scores were averaged and compared between treatment groups as previously reported [37]. Some MFI tissue sections were stained with Prussian Blue for iron localization.

Statistics

Iron concentrations in tissue homogenates were compared between treatment groups by 2-way ANOVA and Sidak's multiple comparison test. Differences in pathology and changes in R2* values were assessed by 2-way ANOVA. Hormone level changes were assessed by 1-way ANOVA.

Results

PBMC Incubations

To determine whether rhesus macaque cells take up ferumoxytol as reported with human cells [14,18-22], prior to initiating the imaging phases of this study, rhesus monocytes, macrophages, and neutrophils were incubated in 100 µg/ml ferumoxytol (Fig. 1), the approximate concentration of ferumoxytol in the blood with administration for MRI, and iron was visualized by Prussian blue staining. Staining was seen in differentiated macrophages but not monocytes or neutrophils. Activation with PMA and ionomycin did not affect iron staining. No staining was seen without ferumoxytol incubation.

Placental Explants Incubations

To determine whether placental ferumoxytol uptake by placental tissue may confound use for inflammation mapping in vivo, prior to initiating the imaging phases of this study, rhesus placental explants were incubated with ferumoxytol and stained with Prussian Blue. Modest background Prussian Blue iron staining in tissue was observed independent of ferumoxytol incubation, likely indicating endogenous iron content (Supplemental Fig. 2). Minimal increase in iron staining was observed after 2 hours of ferumoxytol-incubation. An increase in iron staining appeared after 24 hours incubation, specifically in the villous endothelium of the placental tissue. Not substantial staining of the syncytiotrophoblasts was observed, the primary interface exposed to ferumoxytol in maternal blood in vivo. Low levels of endogenous iron and modest increases in ferumoxytol uptake in control placental explants ex vivo after incubations suggests that in vivo inflammation detection by ferumoxytol-enhanced MRI would be feasible and not confounded by background placental iron content/uptake.

Maternal Clinical Outcomes with Ferumoxytol Administration

In addition to the 7 animals in this study that received ferumoxytol for MRI (Supplemental Fig. 1), 28 pregnant rhesus monkeys from other ongoing studies (unpublished) had up to three ferumoxytol imaging sessions. In 35 total experimental subjects who had ferumoxytol imaging sessions, two animals required moderate medical attention following ferumoxytol administration. Both animals had periocular edema following IV bolus administration of ferumoxytol that was treated with 10 mg diphenhydramine hydrochloride. One animal had a short period of increased heart rate and SPO2 levels. This animal had previous ocular swelling not associated with ferumoxytol, so it is unclear whether this event was due to ferumoxytol or other drugs used to anesthetize the animal. These mild allergic reactions responded to diphenhydramine and the animals recovered without further medical intervention.

Pregnancy Outcomes

Seven pregnant rhesus macaques (Supplemental Fig. 1 A) who underwent MRI gave birth via vaginal delivery at term, and the infants joined the WNPRC colony. Results of these imaging studies are described in separate reports [17,38]. Pregnancy outcomes were generally unremarkable, with one retained placenta (which occurs in ~2.6% of WNPRC pregnancies). None of the seven dams had immediate or long-term reactions to the ferumoxytol treatment.

Infant growth data from these pregnancies are plotted along with their birth year cohort weights (Fig. 2). The weights of the MRI offspring generally stayed within one standard deviation of the average infant weights. Infants followed normal physiological and

sociobehavioral patterns seen in other colony infants as assessed by daily veterinary observations.

Ferumoxytol Detection by MRI Following Administration

Three of the seven pregnant rhesus macaques that carried infants to term (Supplemental Fig. 1 A) had been imaged with ferumoxytol at ~100gd. Imaging occurred immediately before (to establish a baseline R2* values in maternal, MFI, and fetal tissue) and 15 minutes after administration of ferumoxytol, followed by four follow-up MRI scans at approximately one day, one week, two weeks and three weeks following ferumoxytol administration. In all three animals, an increase in R2* values in both the primary and secondary placental disks is seen immediately following ferumoxytol injection (Fig. 3). he R2* values in fetal lung remained close to baseline though all scans while fetal liver R2* values increased slightly in two of the three animals. This may reflect an increase in physiological iron transport to the fetus over time in normal pregnancy, unrelated to ferumoxytol. The R2* values in the placenta, which increased dramatically following ferumoxytol administration, returned to approximate baseline levels within one day post-ferumoxytol, supporting a rapid clearance of ferumoxytol from the blood. Ferumoxytol accumulation in the placenta or transfer to the fetus was not detectable by R2* (Zhu et al, under review).

Iron Content in Tissues

Maternal, MFI, and fetal tissues from 8 pregnancies (Supplemental Fig. 1 B) were surgically collected at ~gd100 following MRI and iron concentrations were determined in these tissues (Fig. 4). When ferumoxytol-exposed and untreated control groups were compared, only

maternal liver showed a significant increase in iron concentration with maternal ferumoxytol administration over control ($p<0.0001$). There are no significant differences in iron in fetal tissues in ferumoxytol vs. non-ferumoxytol-exposed animals.

Prussian Blue Staining of MFI Tissues

Prussian Blue staining varied animal-to-animal in the placenta, decidua, and fetal membranes from animals that underwent fetectomy. Tissues from ferumoxytol-receiving animals, overall, did not have noticeably different staining compared to non-ferumoxytol-receiving animals. Interestingly, the animal with the most consistent staining had not received ferumoxytol (Supplemental Fig. 3), likely reflecting normal physiological iron.

Ferumoxytol Effects on Plasma Progesterone, Estrone, and Estradiol

For each imaging day in animals that underwent fetectomy (Supplemental Fig. 1 B), maternal plasma samples were assessed by mass spectrometry for progesterone, estrone, and estradiol levels [35,36] to assess the impact of MRI imaging and ferumoxytol administration on placental endocrine function. Non-imaged controls (Supplemental Fig. 1 B) received a one-time plasma-collection at time of fetectomy. There was no statistically significant change in placental hormone levels following administration of ferumoxytol and hormone levels generally stayed within the range of levels seen in non-imaged controls (Fig. 5).

Ferumoxytol Effects on Histopathology

Of 37 maternal and fetal tissues collected at fetectomy (Supplemental Data 1), the placenta, decidua, amniotic membranes, placental bed, maternal spleen, and maternal liver had

359 notable histopathology. Animals that did and did not receive ferumoxytol MRI had no

360 statistically significant differences in individual tissue histopathology scores (Fig. 6).

361 Morphologic Diagnoses are provided in Supplemental Data 2.

Discussion

In this study, we examined the impact of MRI with and without ferumoxytol on the fetoplacental and maternal tissues, pregnancy outcomes, and fetal well-being in the pregnant rhesus macaque. Offspring from imaged pregnancies with or without ferumoxytol had uneventful labor and normal growth in comparison with contemporary pregnancies from the WNPRC breeding colony. No significant impact of MRI with ferumoxytol on iron content or histopathology of fetal and MFI tissues (decidua, placenta, fetal membranes) was observed. Placental function as indicated by peripheral blood steroid hormone levels was unaffected by MRI with ferumoxytol. It should be noted that ferumoxytol was injected as a diluted bolus in this study, while it is administered as a slow infusion in humans to reduce the risk of anaphylactic reactions. The lack of significant adverse outcomes in the rhesus subjects also suggests the utility of ferumoxytol as a non-gadolinium contrast agent for MRI in pregnancy studies.

The use of ferumoxytol in MRI of pregnancy has the potential to yield important diagnostic information. Additionally, ferumoxytol-enhanced MR angiography allows for visualization of maternal uteroplacental vessels involved in transporting blood to and from the uterus, and therefore the placenta. When using ferumoxytol as the contrast agent for DCE imaging, the time of arrival of ferumoxytol-laden blood into the intervillous space and perfusion rates of blood into the individual cotyledons can be determined, which may be related to the health of the placental tissue [7,8]. Fetal vessels are not enhanced since significant ferumoxytol does not pass into the fetal circulation during MRI [17], observations further supported by fetal tissue iron data reported here.

We have shown that ferumoxytol is taken up by rhesus monkey phagocytic cells, demonstrating the feasibility of designing additional studies for its application to nonhuman primate models of adverse pregnancy outcomes. Ferumoxytol has not been applied previously to the nonhuman primate model. *In vitro* culture experiments demonstrated that the SPION was taken up by macrophages differentiated from peripheral blood monocytes, but not by undifferentiated monocytes or granulocytes. This indicates that ferumoxytol is a feasible reagent to detect the accumulation of phagocytic macrophages at sites of inflammation. Tissue macrophages take up ferumoxytol and clear these iron nanoparticles more slowly than those in the blood, therefore, sites of inflammation can be located by performing delayed imaging following ferumoxytol administration. This paradigm may help identify inflammation at the MFI, which could predict an insult to the pregnancy.

Concerns about ferumoxytol uptake by the placenta and the potential for transport of elevated levels of iron to the fetus, putting the fetus at risk for hemochromatosis or pulmonary hemosiderosis since these disorders result in fetal growth restriction, hepatic failure, alveolar hemorrhage, and stillbirth [39-41] were addressed. Placental villous explants were incubated *in vitro* with physiologically realistic concentrations of ferumoxytol, and staining of explant tissue sections for iron content with Prussian Blue did not demonstrate any significant uptake of SPION by placental tissues in a physiologically meaningful pattern (i.e., syncytiotrophoblast uptake) that would be anticipated with exposure of the placenta to ferumoxytol in the maternal blood in the intervillous space. With *in vivo* treatment of pregnant rhesus macaques, there was no significant impact on maternal health, pregnancy outcome, or postnatal fetal development. Pilot studies used to establish the parameters for imaging, indicated that offspring from survival pregnancies showed uneventful labor and normal fetal/infant growth compared to contemporary pregnancies

from the WNPRC breeding colony. Furthermore, the dose of ferumoxytol used in these animal studies, while allowing sensitive imaging of the MFI, is quite low (4 mg/kg) compared to human therapeutic dosing for anemia. This underscores the expected safety of ferumoxytol in this pregnancy model.

The fetus acquires iron during pregnancy through transferrin receptor acquisition of ferritin and transit across the placental syncytiotrophoblast and cytotrophoblast to the fetal vasculature within villous stroma [42]. Placental tissues collected from MRI experiments and stained with Prussian Blue for iron content did not reveal discernible differences between tissues from control and ferumoxytol-treated pregnancies. Additionally, decidual tissues and fetal membranes did not demonstrate any consistent differences between experimental groups. There were focally distributed areas of iron detected by Prussian Blue staining, however interestingly, the tissues with the clearest demonstration of iron content were the decidua and fetal membranes rather than the placental villi. It is important to note that the animal in which iron was most readily demonstrated in these tissues did *not* receive ferumoxytol and thus SPION-delivered iron was not the source of Prussian Blue staining. These data suggest that although the placenta directly transports iron to the fetus via a biologically conserved ferritin/ferritin receptor-mediated pathway, this active pathway does not participate in the uptake of ferumoxytol by the syncytiotrophoblasts. While the mechanism of ferumoxytol's uptake by macrophages has not been determined, similar dextran-coated SPIONs are taken up by phagocytosis or SR-A-mediated endocytosis [43-45]. We hypothesize that cellular iron sequestration, as indicated by Prussian Blue staining, may be largely attributable to macrophage uptake of erythrocytes as a routine surveillance function at the MFI.

Consistent with a lack of increase in iron content of MFI tissues by histochemical methods, there was no significant increase in iron concentration in MFI tissues by mass spectrometry. Likewise, fetal tissues that would be anticipated to accumulate iron, did not show a statistically significant increase. While there does appear to be a trend for slightly higher, though not statistically significant, iron content in fetal tissues, further studies will be needed to determine if this is a consistent result. There was a statistically significant increase in maternal liver iron content, which was expected since the liver is a main clearance organ for ferumoxytol, with resident hepatic macrophages (Kupffer cells) taking up ferumoxytol particles in studies in rabbit [46] and human subjects [47,48].

Histopathology was evaluated in selected maternal tissues, the MFI, and in fetal tissues. There was no detectable histopathology in any fetal tissues. While histopathology was noted in tissues at the MFI, there were not significant differences between ferumoxytol-receiving and control animals. Some histopathological features were noted among placentas even in untreated "normal" pregnancies. This lack of a difference in pathological findings in placental, decidual, and fetal membrane specimens from the animals in study also supports the use of ferumoxytol in this animal model. Functional assessment of the placenta by monitoring of placental hormone secretion (progesterone, estradiol, estrone) likewise revealed no significant difference between animals receiving ferumoxytol MRI imaging, and untreated animals.

The data presented in this report were part of a larger study in which some fetuses received IL-1B via an intra-amniotic injection with the goal of inciting trafficking of inflammatory phagocytes to the MFI [29,30]. Ferumoxytol MRI and histochemical and mass spectrometry analyses did not support an increase in iron-retaining cells at the MFI. This previously published model reported increased numbers of macrophages and granulocytes in the

decidua parietalis, however that study did not evaluate the decidua basalis which we hypothesized would be imaged with Ferumoxytol treatment. While our study did not validate the use of Ferumoxytol with this model due to lack of induced inflammation, it is possible that other nonhuman primate models of adverse pregnancy outcomes and MFI inflammation, including maternal infection with *Listeria monocytogenes* [49] or Zika virus [37,50-52] which have been shown to provoke significant inflammation in the decidua basalis with significant placental pathology, may more productively demonstrate the efficacy of ferumoxytol for detection of inflammation at the MFI. Furthermore, a placenta facing a bacterial or viral insult may have altered placental transporter protein expression, which may affect ferumoxytol's ability to pass into the fetal blood circulation [53]. Use of these pregnancy models in ferumoxytol MRI may reveal important experimental utility of the SPION.

The use of an animal model to evaluate MRI methodologies has significant advantages. The pregnant dam is anesthetized for the imaging procedure in the nonhuman primate model, and the inhaled anesthetic is transferred to the fetus, which is also anesthetized. Therefore, the fetal motion is minimized in MRI of the animals, leading to reliable MRI results. This experiment setup provided unique opportunity to validate the feasibility of MRI methodologies without the fetal motion being a confounding factor. However, anesthesia is not the standard of care for MRI evaluation of pregnant humans. The potential fetal motion in MRI of pregnant human subjects need to be addressed. A motion-robust R2* mapping technique has been proposed by our group and is under separate study (Zhu et al, under review). Upon successful validation, the motion-robust MRI technique may enable assessing detection macrophage homing in pregnant women. Other common MRI imaging strategies for motion include motion prevention (e.g. coaching, breath holding), imaging artifact reduction (e.g. physiological

triggering and gating, fast imaging readouts), and motion correction (e.g. navigators, prospective/retrospective corrections) [54]. These, and other strategies, are commonly used in body imaging applications (i.e. cardiac, lung, abdominal) where motion is of substantial concern for producing diagnostic quality MR images..

In summary, we conclude that ferumoxytol administration for imaging in this rhesus pregnancy model is feasible. Future studies will explore the use of ferumoxytol to detect placental inflammation and the diagnostic value of DCE MRI in the presence of placental dysfunction. The rhesus macaque will be an important platform for initial development of novel imaging approaches in an experimentally tractable model.

Acknowledgment

The authors wish to thank GE Healthcare who provides research support to the University of Wisconsin-Madison and AMAG Pharmaceuticals for providing Ferumoxytol for this study. Further, Dr. Reeder is a Romnes Faculty Fellow, and has received an award provided by the University of Wisconsin-Madison Office of the Vice Chancellor for Research and Graduate Education with funding from the Wisconsin Alumni Research Foundation.

References

1. Alexander BT. Placental insufficiency leads to development of hypertension in growth-restricted offspring. Hypertension 2003; 41:457-462.

2. Brosens I, Pijnenborg R, Vercruysse L, Romero R. The "Great Obstetrical Syndromes" are associated with disorders of deep placentation. Am J Obstet Gynecol 2011; 204:193-201.

3. Krishna U, Bhalerao S. Placental insufficiency and fetal growth restriction. J Obstet Gynaecol India 2011; 61:505-511.

4. Roberts DJ, Post MD. The placenta in pre-eclampsia and intrauterine growth restriction. J Clin Pathol 2008; 61:1254-1260.

5. Chalouhi GE, Deloison B, Siauve N, Aimot S, Balvay D, Cuenod CA, Ville Y, Clément O, Salomon LJ. Dynamic contrast-enhanced magnetic resonance imaging: definitive imaging of placental function? Semin Fetal Neonatal Med 2011; 16:22-28.

6. Lohrke J, Frenzel T, Endrikat J, Alves FC, Grist TM, Law M, Lee JM, Leiner T, Li KC, Nikolaou K, Prince MR, Schild HH, et al. 25 Years of Contrast-Enhanced MRI: Developments, Current Challenges and Future Perspectives. Adv Ther 2016; 33:1-28.

7. Frias AE, Schabel MC, Roberts VH, Tudorica A, Grigsby PL, Oh KY, Kroenke CD. Using dynamic contrast-enhanced MRI to quantitatively characterize maternal vascular organization in the primate placenta. Magn Reson Med 2015; 73:1570-1578.

8. Schabel MC, Roberts VHJ, Lo JO, Platt S, Grant KA, Frias AE, Kroenke CD. Functional imaging of the nonhuman primate Placenta with endogenous blood oxygen level-dependent contrast. Magn Reson Med 2016; 76:1551-1562.

9. Siauve N, Chalouhi GE, Deloison B, Alison M, Clement O, Ville Y, Salomon LJ. Functional imaging of the human placenta with magnetic resonance. Am J Obstet Gynecol 2015;

213:S103-114.

10. Rogosnitzky M, Branch S. Gadolinium-based contrast agent toxicity: a review of known and proposed mechanisms. Biometals 2016; 29:365-376.

11. Oh KY, Roberts VH, Schabel MC, Grove KL, Woods M, Frias AE. Gadolinium Chelate Contrast Material in Pregnancy: Fetal Biodistribution in the Nonhuman Primate. Radiology 2015; 276:110-118.

12. Prola-Netto J, Woods M, Roberts VHJ, Sullivan EL, Miller CA, Frias AE, Oh KY. Gadolinium Chelate Safety in Pregnancy: Barely Detectable Gadolinium Levels in the Juvenile Nonhuman Primate after in Utero Exposure. Radiology 2018; 286:122-128.

13. Kanal E, Barkovich AJ, Bell C, Borgstede JP, Bradley WG, Froelich JW, Gimbel JR, Gosbee JW, Kuhni-Kaminski E, Larson PA, Lester JW, Nyenhuis J, et al. ACR guidance document on MR safe practices: 2013. J Magn Reson Imaging 2013; 37:501-530.

14. Bashir MR, Bhatti L, Marin D, Nelson RC. Emerging applications for ferumoxytol as a contrast agent in MRI. J Magn Reson Imaging 2015; 41:884-898.

15. Knobloch G, Colgan T, Wiens CN, Wang X, Schubert T, Hernando D, Sharma SD, Reeder SB. Relaxivity of Ferumoxytol at 1.5 T and 3.0 T. Invest Radiol 2018; 53:257-263.

16. Ludwig KD, Fain SB, Adamson EB, Nguyen S, Golos TG, Reeder SB, Bird IM, Wieben O, Shah DM, Johnson KM. Quantitative ferumoxytol DCE MRI of the primate placental perfusion domains. Proceedings from the 26th Annual Meeting of ISMRM. Paris, France. June 2018.

17. Ludwig KD, Fain SB, Nguyen SM, Golos TG, Reeder SB, Bird IM, Shah DM, Wieben OE, Johnson KM. Perfusion of the placenta assessed using arterial spin labeling and ferumoxytol dynamic contrast enhanced magnetic resonance imaging in the rhesus macaque. Magn Reson

Med 2018.

18. Toth GB, Varallyay CG, Horvath A, Bashir MR, Choyke PL, Daldrup-Link HE, Dosa E, Finn JP, Gahramanov S, Harisinghani M, Macdougall I, Neuwelt A, et al. Current and potential imaging applications of ferumoxytol for magnetic resonance imaging. Kidney Int 2017; 92:47-66.

19. Hasan DM, Amans M, Tihan T, Hess C, Guo Y, Cha S, Su H, Martin AJ, Lawton MT, Neuwelt EA, Saloner DA, Young WL. Ferumoxytol-enhanced MRI to Image Inflammation within Human Brain Arteriovenous Malformations: A Pilot Investigation. Transl Stroke Res 2012; 3:166-173.

20. Iv M, Samghabadi P, Holdsworth S, Gentles A, Rezaii P, Harsh G, Li G, Thomas R, Moseley M, Daldrup-Link HE, Vogel H, Wintermark M, et al. Quantification of Macrophages in High-Grade Gliomas by Using Ferumoxytol-enhanced MRI: A Pilot Study. Radiology 2018:181204.

21. Neuwelt A, Sidhu N, Hu CA, Mlady G, Eberhardt SC, Sillerud LO. Iron-based superparamagnetic nanoparticle contrast agents for MRI of infection and inflammation. AJR Am J Roentgenol 2015; 204:W302-313.

22. Gaglia JL, Harisinghani M, Aganj I, Wojtkiewicz GR, Hedgire S, Benoist C, Mathis D, Weissleder R. Noninvasive mapping of pancreatic inflammation in recent-onset type-1 diabetes patients. Proc Natl Acad Sci U S A 2015; 112:2139-2144.

23. Rozner AE, Dambaeva SV, Drenzek JG, Durning M, Golos TG. Generation of macrophages from peripheral blood monocytes in the rhesus monkey. J Immunol Methods 2009; 351:36-40.

24. Roberts RL, Gallin JI. Rapid method for isolation of normal human peripheral blood

559 eosinophils on discontinuous Percoll gradients and comparison with neutrophils. Blood 1985;
560 65:433-440.
561 25. Sheehan D, Hrapchak B. Theory and practice of Histotechnology, 2nd Ed, 1980, pp217-
562 218, Battelle Press, Ohio.
563 26. Luna L. Manual of Histologic Staining Methods of the AFIP, 3rd Ed, 1968, pp 183,
564 McGraw-Hill, NY.
565 27. Crookham J, Dapson R. Hazardous Chemicals in the Histopathology Laboratory, 2nd
566 ED, 1991, Anatech.
567 28. Tarantal AF. Ultrasound Imaging in Rhesus (Macaca mulatta) and Long-tailed (Macaca
568 fascicularis) Macaques: Reproductive and Research Applications. In: Wolfe-Coote S, editor. The
569 Laboratory Primate. London: Elsevier; 2005. p. 317–52.
570 29. Presicce P, Senthamaraikannan P, Alvarez M, Rueda CM, Cappelletti M, Miller LA, Jobe
571 AH, Chougnet CA, Kallapur SG. Neutrophil recruitment and activation in decidua with intra-
572 amniotic IL-1beta in the preterm rhesus macaque. Biol Reprod 2015; 92:56.
573 30. Kallapur SG, Presicce P, Senthamaraikannan P, Alvarez M, Tarantal AF, Miller LM,
574 Jobe AH, Chougnet CA. Intra-amniotic IL-1β induces fetal inflammation in rhesus monkeys and
575 alters the regulatory T cell/IL-17 balance. J Immunol 2013; 191:1102-1109.
576 31. Krynitsky AJ. Preparation of Biological Tissue for the Determination of Arsenic and
577 Selenium by Graphite Furnace Atomic Absorption Spectrometry. Anal. Chem., Vol. 59, pp
578 1884-1886. (1987).
579 32. Giesy JP, Wagner JG. Frequency Distributions of Trace Metal Concentrations in Five
580 Freshwater Fishes. Trans. Am. Fis. Soc., Vol. 106, No. 4, pp 393-403. (1977),
581 33. Test Methods for Evaluating Solid Waste Physical/Chemical Methods. Third edition,

582 SW-846, USEPA. November 1986, including July 1992, August 1993, September 1994, and
583 January 1995 updates. Method 6010B.
584 34. Methods for the Determination of Metals in Environmental Samples. USEPA, 200.7,
585 1994.
586 35. Kenealy BP, Kapoor A, Guerriero KA, Keen KL, Garcia JP, Kurian JR, Ziegler TE,
587 Terasawa E. Neuroestradiol in the hypothalamus contributes to the regulation of gonadotropin
588 releasing hormone release. J Neurosci 2013; 33:19051-19059.
589 36. Kenealy BP, Keen KL, Kapoor A, Terasawa E. Neuroestradiol in the Stalk Median
590 Eminence of Female Rhesus Macaques Decreases in Association With Puberty Onset.
591 Endocrinology 2016; 157:70-76.
592 37. Nguyen SM, Antony KM, Dudley DM, Kohn S, Simmons HA, Wolfe B, Salamat MS,
593 Teixeira LBC, Wiepz GJ, Thoong TH, Aliota MT, Weiler AM, et al. Highly efficient maternal-
594 fetal Zika virus transmission in pregnant rhesus macaques. PLoS Pathog 2017; 13:e1006378.
595 38. Macdonald JA, Corrado PA, Nguyen SM, Johnson KM, Francois CJ, Magness RR, Shah
596 DM, Golos TG, Wieben O. Uteroplacental and Fetal 4D Flow MRI in the Pregnant Rhesus
597 Macaque. J Magn Reson Imaging 2018.
598 39. Kelly AL, Lunt PW, Rodrigues F, Berry PJ, Flynn DM, McKiernan PJ, Kelly DA, Mieli-
599 Vergani G, Cox TM. Classification and genetic features of neonatal haemochromatosis: a study
600 of 27 affected pedigrees and molecular analysis of genes implicated in iron metabolism. J Med
601 Genet 2001; 38:599-610.
602 40. Fellman V, Rapola J, Pihko H, Varilo T, Raivio KO. Iron-overload disease in infants
603 involving fetal growth retardation, lactic acidosis, liver haemosiderosis, and aminoaciduria.
604 Lancet 1998; 351:490-493.

605 41. Limme B, Nicolescu R, Misson JP. Neonatal pulmonary hemosiderosis. Case Rep Pediatr
606 2014; 2014:463973.
607 42. Fuchs R, Ellinger I. Endocytic and transcytotic processes in villous syncytiotrophoblast:
608 role in nutrient transport to the human fetus. Traffic 2004; 5:725-738.
609 43. Corot C, Robert P, Idée JM, Port M. Recent advances in iron oxide nanocrystal
610 technology for medical imaging. Adv Drug Deliv Rev 2006; 58:1471-1504.
611 44. Raynal I, Prigent P, Peyramaure S, Najid A, Rebuzzi C, Corot C. Macrophage
612 endocytosis of superparamagnetic iron oxide nanoparticles: mechanisms and comparison of
613 ferumoxides and ferumoxtran-10. Invest Radiol 2004; 39:56-63.
614 45. Feng Q, Liu Y, Huang J, Chen K, Xiao K. Uptake, distribution, clearance, and toxicity of
615 iron oxide nanoparticles with different sizes and coatings. Sci Rep 2018; 8:2082.
616 46. Yancy AD, Olzinski AR, Hu TC, Lenhard SC, Aravindhan K, Gruver SM, Jacobs PM,
617 Willette RN, Jucker BM. Differential uptake of ferumoxtran-10 and ferumoxytol, ultrasmall
618 superparamagnetic iron oxide contrast agents in rabbit: critical determinants of atherosclerotic
619 plaque labeling. J Magn Reson Imaging 2005; 21:432-442.
620 47. Lim JH, Choi D, Cho SK, Kim SH, Lee WJ, Lim HK, Park CK, Paik SW, Kim YI.
621 Conspicuity of hepatocellular nodular lesions in cirrhotic livers at ferumoxides-enhanced MR
622 imaging: importance of Kupffer cell number. Radiology 2001; 220:669-676.
623 48. Ramanathan RK, Korn RL, Raghunand N, Sachdev JC, Newbold RG, Jameson G,
624 Fetterly GJ, Prey J, Klinz SG, Kim J, Cain J, Hendriks BS, et al. Correlation between
625 Ferumoxytol Uptake in Tumor Lesions by MRI and Response to Nanoliposomal Irinotecan in
626 Patients with Advanced Solid Tumors: A Pilot Study. Clin Cancer Res 2017; 23:3638-3648.
627 49. Wolfe B, Wiepz GJ, Schotzko M, Bondarenko GI, Durning M, Simmons HA, Mejia A,

628 Faith NG, Sampene E, Suresh M, Kathariou S, Czuprynski CJ, et al. Acute Fetal Demise with
629 First Trimester Maternal Infection Resulting from *Listeria monocytogenes* in a Nonhuman
630 Primate Model. MBio 2017; 8.
631 50. Mohr EL, Block LN, Newman CM, Stewart LM, Koenig M, Semler M, Breitbach ME,
632 Teixeira LBC, Zeng X, Weiler AM, Barry GL, Thoong TH, et al. Ocular and uteroplacental
633 pathology in a macaque pregnancy with congenital Zika virus infection. PLoS One 2018;
634 13:e0190617.
635 51. Dudley DM, Aliota MT, Mohr EL, Weiler AM, Lehrer-Brey G, Weisgrau KL, Mohns
636 MS, Breitbach ME, Rasheed MN, Newman CM, Gellerup DD, Moncla LH, et al. A rhesus
637 macaque model of Asian-lineage Zika virus infection. Nat Commun 2016; 7:12204.
638 52. Hirsch AJ, Roberts VHJ, Grigsby PL, Haese N, Schabel MC, Wang X, Lo JO, Liu Z,
639 Kroenke CD, Smith JL, Kelleher M, Broeckel R, et al. Zika virus infection in pregnant rhesus
640 macaques causes placental dysfunction and immunopathology. Nat Commun 2018; 9:263.
641 53. Lye P, Bloise E, Javam M, Gibb W, Lye SJ, Matthews SG. Impact of bacterial and viral
642 challenge on multidrug resistance in first- and third-trimester human placenta. Am J Pathol 2015;
643 185:1666-1675.
644 54. Zaitsev M, Maclaren J, Herbst M. Motion artifacts in MRI: A complex problem with
645 many partial solutions. J Magn Reson Imaging 2015; 42:887-901.

Figure Legends

Fig. 1. Localization of iron in rhesus immune cells incubated with ferumoxytol. Peripheral blood neutrophils (left), monocytes (center), and *in vitro*-differentiated macrophages (right) from rhesus macaque whole blood were incubated in 100 µg/ml ferumoxytol for 1 hour and stained with Prussian Blue. Photomicrographs are of cytospins of neutrophils, or monocytes or macrophages grown on coverslips in culture.

Fig. 2. Infant growth rates with maternal ferumoxytol treatment compared to animal colony controls. The black line represents the mean weight (kg) for 116 infants born at the WNPRC in 2016, weighed at the age in days listed on the x-axis. The grey lines represent one standard deviation from the mean. Purple lines represent one animal each that was imaged by MRI without ferumoxytol. Aqua lines represent one animal each that was imaged with ferumoxytol, plus 4 additional scans without additional ferumoxytol administration. The irregular mean and standard deviation lines reflect the fact that not all colony animals were weighted on any given day so the data represent a different population of animals at any specific time point.

Fig. 3. R2* values following ferumoxytol injection. R2* values were monitored in 3 pregnant rhesus macaques immediately following and 1 day, 1 week, 2 weeks, and 3 weeks ferumoxytol injection. The image on the top right is a representative Dynamic Contrast Enhanced (DCE) image of maternal and uterine ferumoxytol detection, including placental intervillous flow, illustrating the imaging data used to determine R2* values. The first point represents pre-injection (“0, pre-feru”) and the second point represents the same day post-injection (“0, post-

669 feru"). Primary placental disc values are in dark blue, secondary placenta in aqua, fetal lung in
670 orange, and fetal liver in green.
671
672 **Fig. 4. Iron content of maternal and fetal tissues.** Iron content of selected tissues was
673 determined by mass spectrometry. Non-imaged animals are represented by grey circles (n=4).
674 Animals that received ferumoxytol imaging with intra-amniotic saline are in blue (n=4, except
675 for maternal liver and maternal spleen where n=3). Mean and standard error are denoted by
676 horizontal lines for each tissue.
677
678 **Fig. 5. Plasma hormone levels in MRI animals assessed by mass spectrometry.** Blue lines
679 represent progesterone, estrogen, and estradiol levels in ferumoxytol-infused animals before
680 injection, 24h following injection, and 48h or 72h following injection. Black plus signs (+)
681 represent single blood draw readings from non-ferumoxytol control animals, indicating the
682 expected range of peripheral blood steroid hormone levels in pregnant macaques.
683
684 **Fig. 6. Chart summarizing histopathology scores of all tissues that showed pathology.** For
685 each animal, the circle representing each tissue is colored to denote severity of pathology. The
686 top 4 rows represent the ferumoxytol-receiving intra-amniotic saline animals and the bottom 4
687 rows are for non-ferumoxytol non-MRI controls. Numbers were assigned to each severity rating
688 and used to analyze pathologies (normal=0, minimal=1, mild=2, moderate=3, severe=4). The
689 chart below presents the average pathology scores for each tissue per treatment, used to assess
690 statistical significance.
691

692 **Supplemental Data Legends**

693 **Supplemental Fig. 1. Experimental Design.** Monkey outlines represent a single animal that
694 received each treatment, represented on their respective timeline. (A) Blue timelines outline
695 experimental design for animals where pregnancy proceeded to term and the infants were born
696 by spontaneous vaginal delivery. (B) Pink timelines outline the series of procedures that animals
697 received whose pregnancies were terminated by fetectomy. IA=intra-amniotic, FTX=fetectomy.
698
699 **Supplemental Fig. 2. Histological analysis of rhesus placental explants.** Placental explants
700 from tissue from first (left column) and third (right column) trimester pregnancies were
701 incubated in ferumoxytol for 2 and 24 hours (200 µg/ml ferumoxytol for first trimester, 100
702 µg/ml ferumoxytol for third trimester). Original experiments were at the 200 µg/ml
703 concentration but changed to 100 µg/ml as this concentration better reflects the concentration of
704 ferumoxytol in the blood when imaging. Tissue explants were embedded in paraffin and sections
705 were cut and stained with Prussian Blue to localize iron. The top row shows control tissue that
706 was not incubated in ferumoxytol. The middle row shows the 2 hour incubation. The bottom row
707 shows the 24 hour incubation.
708
709 **Supplemental Fig. 3. Histochemical analysis of iron at the MFI.** The left image presents a
710 representative chorioamniotic membrane sample stained with Prussian Blue, the right image
711 presents a full-thickness placental section (with decidua and membranes attached) similarly
712 stained. Both samples were collected from a non-MRI, non-ferumoxytol control animal. The
713 lower panels present a higher magnification view of the regions depicted by rectangles in the
714 upper panels. These images are from an animal that did not receive ferumoxytol, the degree of

Prussian Blue staining was not seen to increase in animals that received ferumoxytol (not shown).

Supplemental Data 1. Tissues Collected at Fetectomy. The table presents the tissues collected from dams and fetuses at fetectomy after ferumoxytol MRI, or from untreated pregnancies.

Supplemental Data 2. Pathology Reports. The table describes full pathology reports for the tissues summarized in Fig. 6.

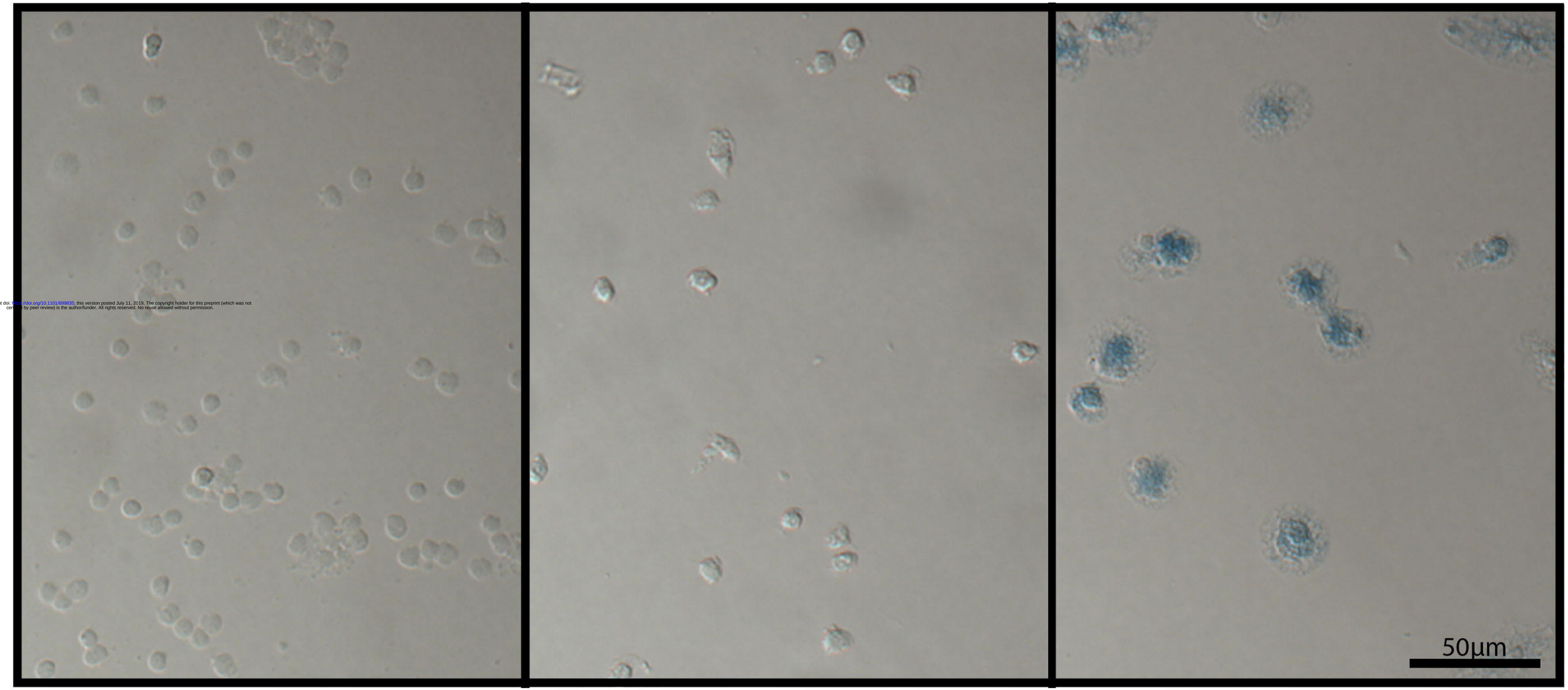

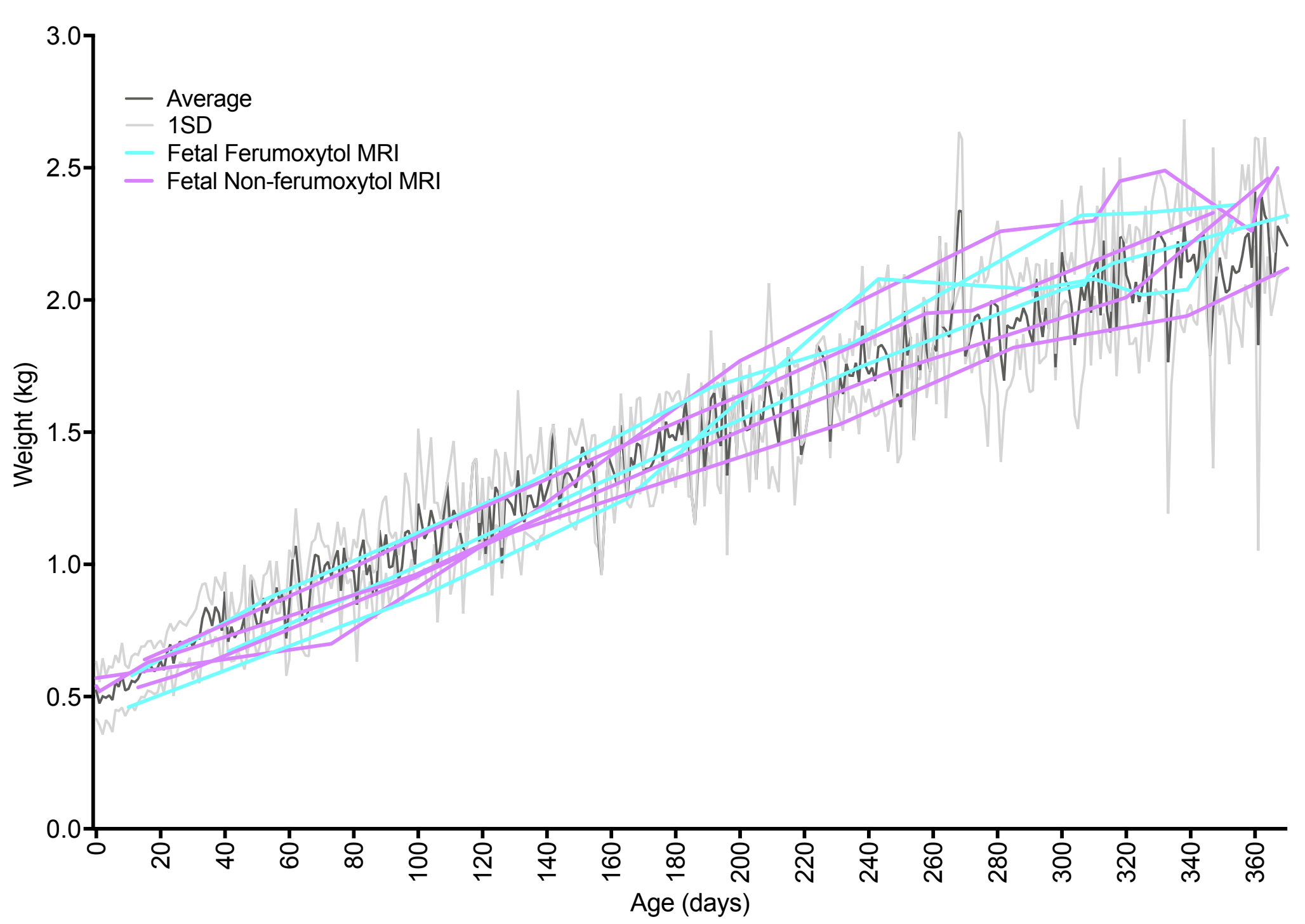
Average
1SD
Fetal Ferumoxytol MRI
Fetal Non-ferumoxytol MRI
Weight (kg)
3.0
2.5
2.0
1.5
1.0
0.5
0.0
0
20
40
60
80
100
120
140
160
180
200
220
240
260
280
300
320
340
360
Age (days)

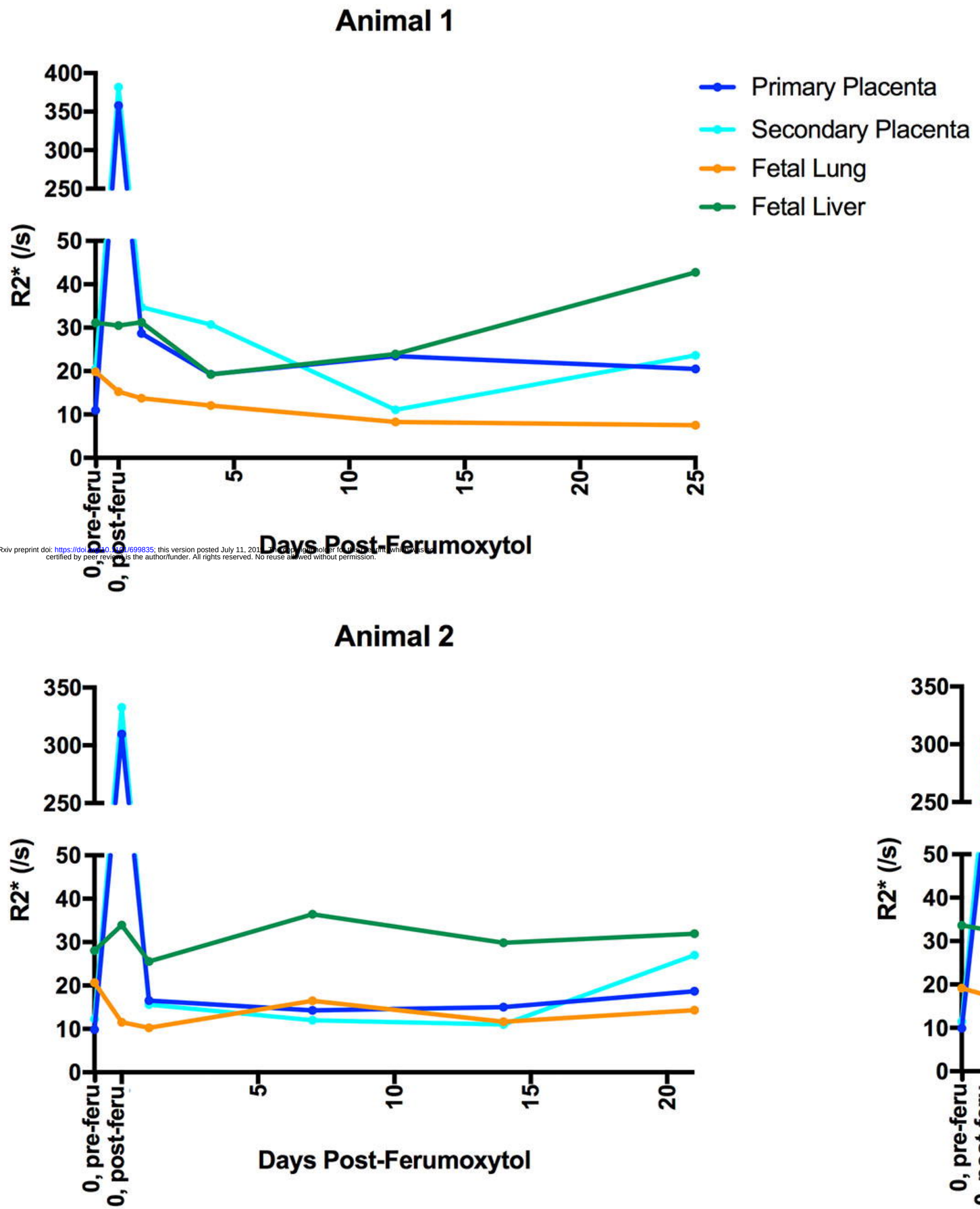

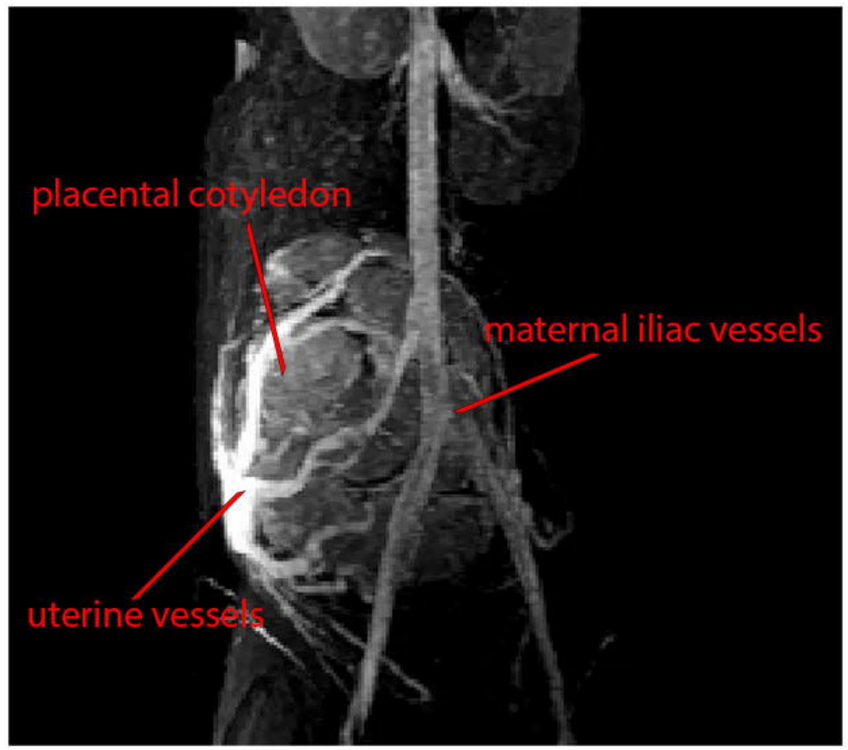

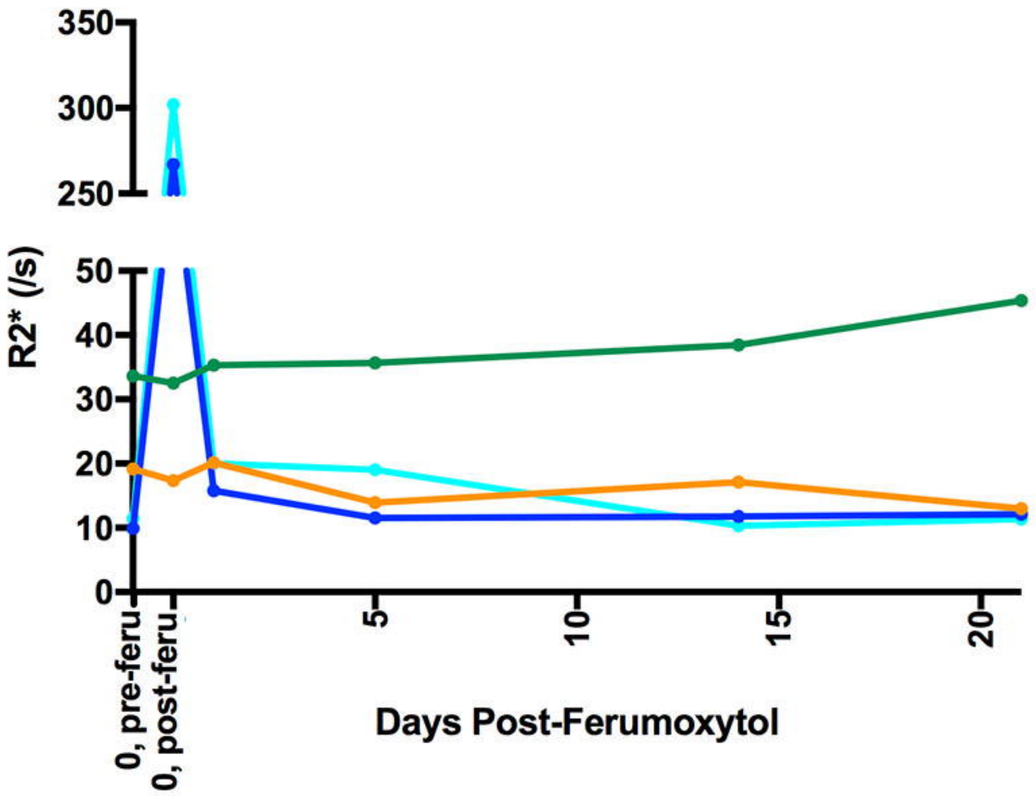

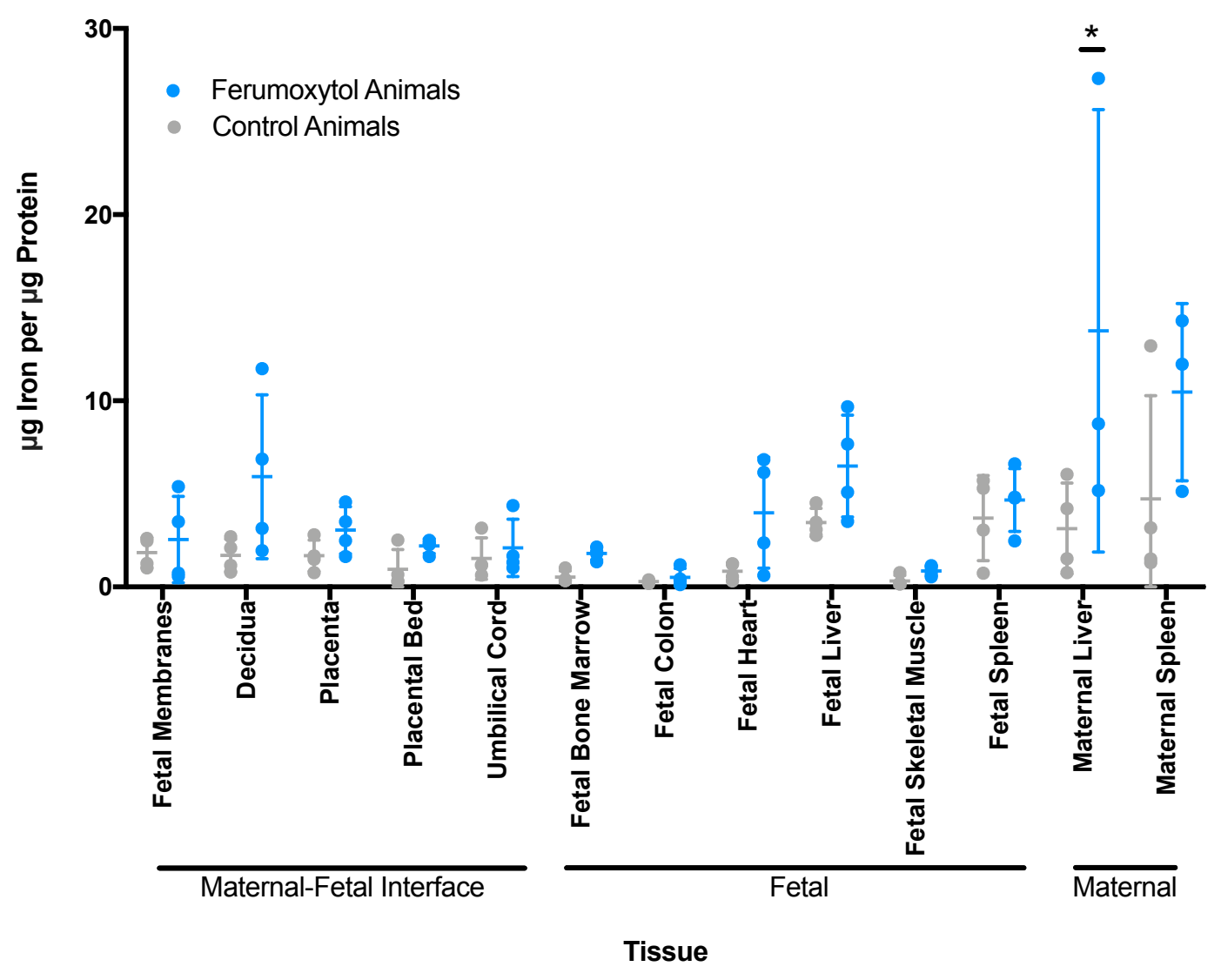
30
20
10
0
µg Iron per µg Protein
Ferumoxytol Animals
Control Animals
*
Fetal Membranes
Decidua
Placenta
Placental Bed
Umbilical Cord
Fetal Bone Marrow
Fetal Colon
Fetal Heart
Fetal Liver
Fetal Skeletal Muscle
Fetal Spleen
Maternal Liver
Maternal Spleen
Maternal-Fetal Interface
Fetal
Maternal
Tissue

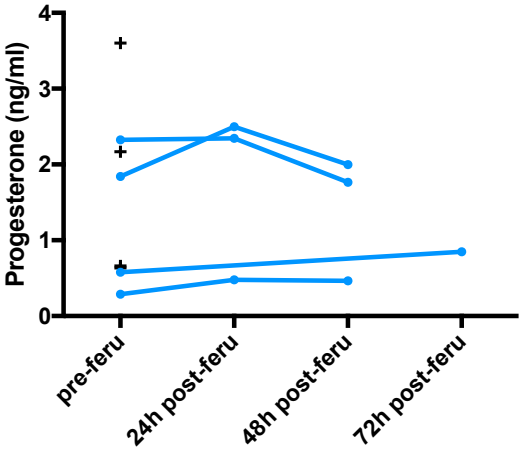
Progesterone (ng/ml)
4
3
2
1
0
pre-feru
24h post-feru
48h post-feru
72h post-feru

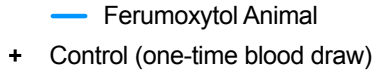
Ferumoxytol Animal
Control (one-time blood draw)

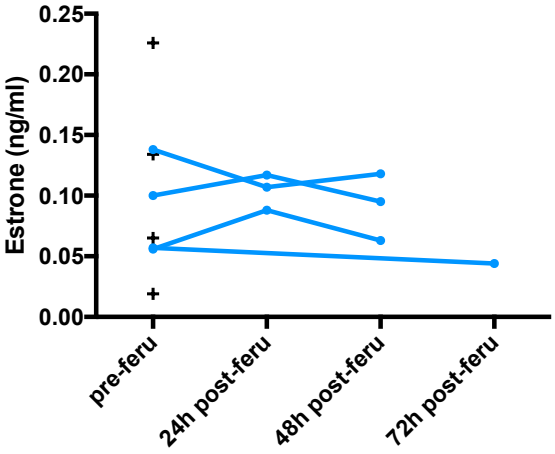
Estrone (ng/ml)
0.25
0.20
0.15
0.10
0.05
0.00
pre-feru
24h post-feru
48h post-feru
72h post-feru

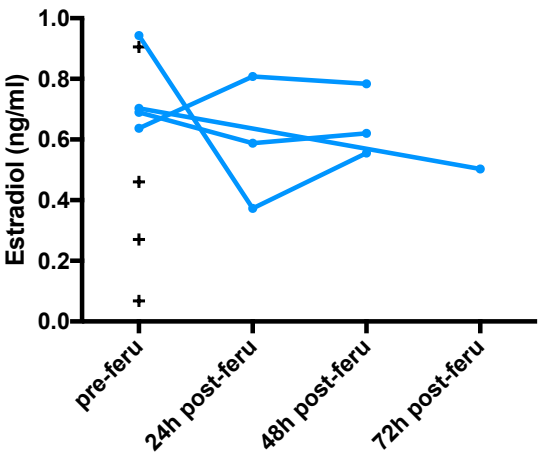
Estradiol (ng/ml)
1.0
0.8
0.6
0.4
0.2
0.0
pre-feru
24h post-feru
48h post-feru
72h post-feru

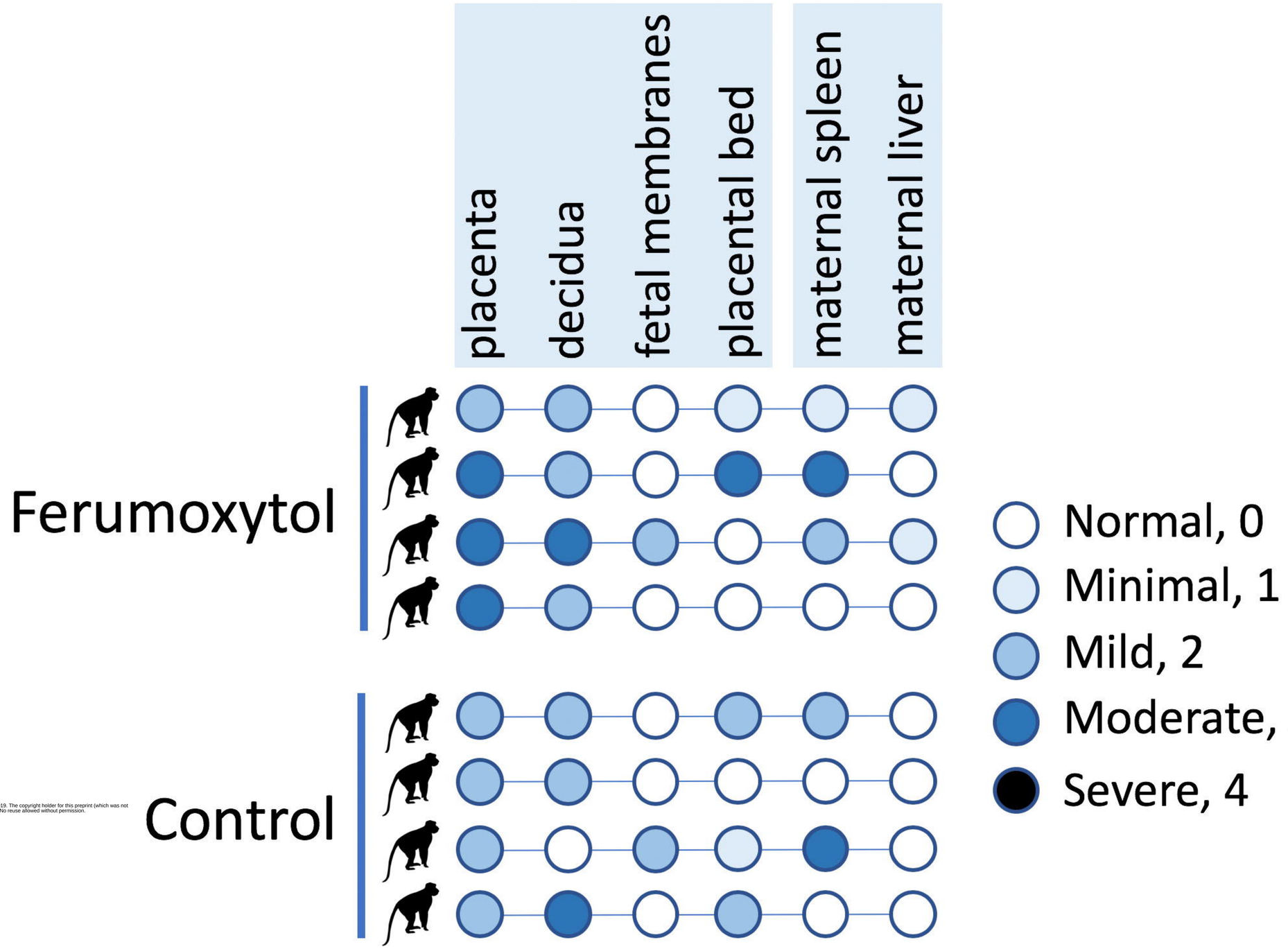

Average Pathology Scores with Standard Error

	Placenta	Decidua	Fetal Membranes	Placental Bed	Maternal Spleen	Maternal Liver
Ferumoxytol	2.75±0.25	2.25±0.25	0.5±0.5	1±0.71	1.5±0.65	0.5±0.29
Control	2±0	1.75±0.63	0.5±0.5	1.25±0.48	1.25±0.75	0±0